Functional Compensation Among HMGN Variants Modulates the DNase I Hypersensitive Sites at Enhancers

Tao Deng[1#], Z. Iris Zhu[2#], Shaofei Zhang[1], Yuri Postnikov[1], Di Huang[2], Marion Horsch[3], Takashi Furusawa[1], Johannes Beckers[3,5,10], Jan Rozman[3,10], Martin Klingenspor[3,4], Oana Amarie[3,11], Jochen Graw[3,11], Birgit Rathkolb[3,10], Eckhard Wolf[5], Thure Adler[3], Dirk H. Busch[6] Valérie Gailus-Durner[3,9], Helmut Fuchs[3], Martin Hrabě de Angelis[3,9,10], Arjan van der Velde[2,7], Lino Tessarollo[8], Ivan Ovcherenko[2], David Landsman[2] and Michael Bustin[1]*

[1]Protein Section, Laboratory of Metabolism, Center for Cancer Research, National Cancer Institute, National Institutes of Health, Bethesda, MD 20892, [2]Computational Biology Branch, National Center for Biotechnology Information, National Library of Medicine, Bethesda, MD 20892, [3]German Mouse Clinic, Institute of Experimental Genetics, Helmholtz Zentrum München, German Research Center for Environmental Health, Ingolstädter Landstraße 1, 85764 Neuherberg, Germany, [4] Chair of Molecular Nutritional Medicine, Technische Universität München, 85350 Freising, Germany, [5] Ludwig-Maximilians-Universität München, Gene Center, Institute of Molecular Animal Breeding and Biotechnology, Feodor-Lynen Strasse 25, 81377 Munich, Germany, [6] Institute for Medical Microbiology, Immunology and Hygiene, Technische Universität München, Trogerstrasse 30, 81675 Munich, Germany, [7]current address: Bioinformatics Program, Boston University, Boston, MA 02215, Center for Nutrition and Food Sciences, Technische Universität München, 85350 Freising, Germany, [8]Neural Development Section, Mouse Cancer Genetics Program, National Cancer Institute, Frederick, MD, 21702. [9]Chair of Experimental Genetics, Center of Life and Food Sciences Weihenstephan, Technische Universität München, 85354 Freising-Weihenstephan, Germany, [10]Member of German Center for Diabetes Research (DZD), Ingolstädter Landstraße 1, 85764 Neuherberg, Germany, [11]Institute of Developmental Genetics (IDG), Ingolstädter Landstrasse 1, 85764 Neuherberg, Germany.

Running title: HMGN variants maintain DNase I sites

# equal contributions

*Corresponding author: Bldg 37 Room 3122, 37 Convent Drive, Bethesda, MD 20892, US

Email: bustinm@mail.nih.gov

Manuscripts\2015_Revised_Final_Rev-2

SUMMARY

DNase I hypersensitive sites (DHSs) are a hallmark of chromatin regions containing regulatory DNA such as enhancers and promoters; however, the factors affecting the establishment and maintenance of these sites are not fully understood. We now show that HMGN1 and HMGN2, nucleosome-binding proteins that are ubiquitously expressed in vertebrate cells, maintain the DHSs landscape of mouse embryonic fibroblasts (MEFs) synergistically. Loss of one of these HMGN variants led to a compensatory increase of binding of the remaining variant. Genome wide mapping of the DHSs in $Hmgn1^{-/-}$, $Hmgn2^{-/-}$ and $Hmgn1^{-/-}n2^{-/-}$ MEFs reveals that loss of both, but not a single HMGN variant, leads to significant remodeling of the DHSs landscape, especially at enhancer regions marked by H3K4me1 and H3K27ac. Loss of HMGN variants affects the induced expression of stress responsive genes in MEFs, the transcription profiles of several mouse tissues, and leads to altered phenotypes that are not seen in mice lacking only one variant. We conclude that the compensatory binding of HMGN variants to chromatin maintains the DHSs landscape and the transcription fidelity and is necessary to retain wild type phenotypes. Our study provides insights into mechanisms that maintain regulatory sites in chromatin and into functional compensation among nucleosome binding architectural proteins.

INTRODUCTION

Tissue and developmental specific gene expression is facilitated by the binding of transcription factors to unique DNA sequences at regulatory sites in chromatin, such as enhancers and promoters. At these sites, the organization of the nucleosomes is altered, rendering the DNA more accessible to regulatory factors and hypersensitive to digestion by various nucleases including DNase I. DNase I hypersensitive sites (DHSs) are a hallmark of chromatin regions containing regulatory DNA and are used to identify regulatory sites in chromatin. The DHSs chromatin landscape is cell-type specific and dynamic, reflecting changes in the cellular transcription profile occurring during development, or as a consequence of genomic changes leading to altered cellular phenotypes (Gross and Garrard 1988; Boyle et al. 2008; Thurman et al. 2012; Calo and Wysocka 2013; Stergachis et al. 2013).

The molecular mechanisms that establish and maintain DHSs and their role in gene expression are key questions in chromatin biology. DHSs are established by the combined action of transcription factors that bind dynamically to specific DNA sequences, and of chromatin remodeling complexes that alter the organization of the nucleosomes at these sites. Chromatin dynamics play an important role in the plasticity of the DHSs landscape since it affects the ability of transcription factors to access potential new regulatory sites and facilitate the loss of unused sites. Although DHSs are stable and perpetuated to daughter cells, they are not necessarily static; they are maintained by a steady state, rapid, and continuous turnover of regulatory factors at specific sites (Narlikar et al. 2002; Erdel and Rippe 2011; Wippo et al. 2011; Calo and Wysocka 2013; Mueller-Planitz et al. 2013; Swygert and Peterson 2014; Voss and Hager 2014).

Given the dynamic nature of the DHSs, it could be expected that nucleosome binding proteins known to affect chromatin compaction and accessibility, such as linker histone H1 variants, or members of the high mobility group (HMG) families, could play a role in establishing or maintaining the DHSs landscape, a possibility that has not yet been examined. The three distinct families of HMG proteins named HMGA, HMGB and HMGN, are each characterized by a specific functional domain (Bustin 1999; Bianchi and Agresti 2005). The HMGN family is unique in its ability to bind specifically to the 147 base pair nucleosome core particle, but not to purified DNA (Bustin 1999; Bianchi and Agresti 2005). HMGNs have been shown to bind to chromatin with a short residence time, efficiently counteract the chromatin condensing activity of histone H1 and induce changes in chromatin structure (Bustin 2001; Rochman et al. 2009). Chromatin immunoprecipitation studies revealed that HMGN1, one of the two major HMGN variants, colocalizes genome wide with DHSs, (Cuddapah et al. 2011; Deng et al. 2013) however it is not clear whether HMGNs affect the organization of DHSs in chromatin.

Here we examine the role of HMGN1 and HMGN2, the predominant variants of the HMGN nucleosome binding protein family, in modulating the DHSs landscape of mouse embryonic fibroblasts (MEFs). HMGN1 and HMGN2 are widely expressed in vertebrate cells and compete for nucleosome binding sites (Bustin 2001; Catez et al. 2002; Ueda et al. 2008)(Bustin 2001; Catez et al. 2002; Ueda et al. 2008), raising the possibility of functional redundancy among these variants. Therefore we generated $Hmgn2^{-/-}$ mice and mated them with $Hmgn1^{-/-}$ mice to obtain $Hmgn1^{-/-}/n2^{-/-}$ mice, lacking both variants. We prepared MEFs from the three mouse strains and used genome wide approaches and transcriptional analyses to examine whether the highly conserved HMGN nucleosome binding architectural proteins impact

4

chromatin organization and gene expression. To gain insights into the biological function of the proteins in the contexts of an entire organism, we subjected the mice to a battery of phenotypic tests.

Our studies provide new insights into the biological function and mechanism of action of a ubiquitous family of chromatin binding architectural proteins.

RESULTS

Compensatory binding of HMGN1 and HMGN2 to chromatin.

HMGN1 and HMGN2 are the major variants of the HMGN protein family that is ubiquitously expressed in vertebrate cells (Bustin 2001). Since the HMGN1 variant localizes with DHSs in both human T cells and mouse neuroprogenitors (NPs), we examined the genome wide organization of the HMGN2 variant in NPs. We identified 21,600 HMGN2 binding sites; 15,000 (74%) of these sites colocalized with DHSs showing a Pearson correlation coefficient of 0.91 (Fig. 1A). The HMGN2 distribution across the genome was similar to that of HMGN1; we find that 16,500 (76%) of the HMGN2 sites overlapped with HMGN1 sites (Fig. 1B) showing a Pearson correlation coefficient of 0.66 (Fig. 1C).

Given the extensive co-localization between the HMGN variants we tested for possible interplay between these variants by examining the genome wide organization of HMGN2 in NPs lacking HMGN1 ($Hmgn1^{-/-}$ NPs). In $Hmgn1^{-/-}$ NPs we detect 39,700 HMGN2 binding sites, an 80% increase as compared to the number of binding sites in wild type NPs (Fig. 1B). Compared to WT cells, in $Hmgn1^{-/-}$ NPs, the occupancy of HMGN2 did not change significantly at sites that were shared with HMGN1 (Fig. 1D), but it significantly increased at sites that were exclusively occupied by HMGN1 (Fig. 1E), and decreased at sites that were exclusively occupied only by

HMGN2 (Fig. 1F). Thus, loss of the HMGN1 variant increases the chromatin occupancy of HMGN2 (Fig. 1G), raising the possibility of functional compensation among these two major HMGN variants.

To test for possible functional compensation between the HMGN variants we generated $Hmgn2^{-/-}$ mice (Fig. S1A-D) and mated them with $Hmgn1^{-/-}$ mice (Birger et al. 2003) to obtain $Hmgn1^{-/-}/n2^{-/-}$ mice, lacking both variants (Fig. S1E). We derived mouse embryonic fibroblasts (MEFs) from 13.5 day old embryos of $Hmgn1^{-/-}$, $Hmgn2^{-/-}$, and $Hmgn1^{-/-}/n2^{-/-}$ mice and used these cells to examine whether HMGN variants affect the organization of regulatory sites in chromatin.

Chromatin immunoprecipitation analyses indicated that the antibodies to either HMGN1 or HMGN2 specifically recognize the chromatin bound HMGNs since the amount of chromatin immunoprecipitated by anti HMGN1 from WT MEFs was 18 times higher than the amount of chromatin precipitated from $Hmgn1^{-/-}$ MEFs. Similarly, the anti HMGN2 antibodies immunoprecipitated 22 fold more chromatin from WT MEFs as compared to $Hmgn2^{-/-}$ MEFs (Fig. 2A). Significantly, compared with WT MEFs, anti HMGN2 antibody immunoprecipitated twice as much chromatin from $Hmgn1^{-/-}$ MEFs, while anti HMGN1 immunoprecipitated twice as much chromatin from $Hmgn2^{-/-}$ cells (Fig. 2A). Thus, loss of HMGN1 increases the amount of chromatin-bound HMGN2, while loss of HMGN2 increases the amount of chromatin-bound HMGN1; a finding fully compatible with the analysis of HMGN2 organization in NPs and with previous FRAP analyses of living cells which demonstrated competition among HMGN variants for chromatin binding sites (Catez et al. 2002). Taken together, the results suggest that loss of an HMGN variant is compensated by increased chromatin binding of the remaining variant.

6

Synergistic effects of HMGN variants on the DHSs landscape of MEFs.

DNase I hypersensitivity mapping identified 102,034 DHSs in wild type (WT) MEFs, 101,159 sites in $Hmgn1^{-/-}$ MEFs, and 107,150 sites in $Hmgn2^{-/-}$ MEFs, with an 80% of overlap between WT and each of the $Hmgn^{-/-}$ cells (Fig. 2B,C). The DHSs distribution and intensity across the genome was not significantly affected by loss of a single HMGN variant; the Pearson correlation coefficient between WT and either $Hmgn1^{-/-}$ or $Hmgn2^{-/-}$MEFs was 0.86 and 0.93, respectively (Fig. 2E,F), similar to that of two biological replicates of the same genotype (Fig. S2).

While loss of a single HMGN variant did not affect significantly the DHSs landscape, loss of both HMGN variants did alter the DHSs landscape. We identified only 67,363 DHSs in $Hmgn1^{-/-}n2^{-/-}$ MEFs; of these 57% overlapped with DHSs seen in WT MEFs and 43% were newly formed. Thus, over 60% of the DHSs identified in WT cells were lost in $Hmgn1^{-/-}n2^{-/-}$ (Fig. 2D). The correlation plot of the overall DHSs intensity between WT and $Hmgn1^{-/-}n2^{-/-}$ MEFs shows a high scatter with a Pearson correlation coefficient of 0.65 (Fig. 2G). The genomic snapshot shown in Fig. 2K visualizes the significant loss and gain of DHSs in $Hmgn1^{-/-}n2^{-/-}$ as compared to WT, $Hmgn1^{-/-}$ or $Hmgn2^{-/-}$ MEFs. Thus, the combined loss of HMGN1 and HMGN2 led to both loss and gain of DHSs, suggesting that the proteins synergistically remodeled the DHSs landscape of MEFs.

Loss of both HMGN variants affected not only the number of sites detected but also significantly decreased the width of the remaining DHSs, as measured by the amount of base pairs encompassed in a site. Thus, in $Hmgn1^{-/-}n2^{-/-}$ MEFs, the median DHS width is only half of that in WT cells (Fig. 2H) and the total genomic region covered by DHS in $Hmgn1^{-/-}n2^{-/-}$ MEFs is less than half of that covered in WT cells (Fig. S3A, all DHSs). This trend was even more

pronounced when the width of the sites that were present in WT but absent in $Hmgn1^{-/-}n2^{-/-}$ MEFs (black in Fig. 2D) is compared to the sites that were absent in WT but present in $Hmgn1^{-/-}$ $n2^{-/-}$ MEFs (red in Fig. 2D): the median width of lost DHSs was 2.5 times larger than the newly formed, gained sites in $Hmgn1^{-/-}n2^{-/-}$ cells (Fig. 2I), and the total genomic region covered by unique peaks in WT cells was 4 times larger than in $Hmgn1^{-/-}n2^{-/-}$ MEFs (Fig. S3A, unique DHSs). Likewise, the shared sites, although present both in WT and $Hmgn1^{-/-}n2^{-/-}$ MEFs (white in Fig. 2D) showed a similar effect; the median width of these sites decreased from 2000bp in WT to 800bp in $Hmgn1^{-/-}n2^{-/-}$ MEFs (Fig. 2J, Fig. S3A-shared DHSs). Furthermore, to avoid the potential issue that the peak calling software may not accurately assess the width of a peak, we also plotted the aggregate DHS accessibility around all the peaks in WT and $Hmgn1^{-/-}n2^{-/-}$ MEFs. The results indicate that indeed, the average half height width of the DNase I peak in $Hmgn1^{-/-}n2^{-/-}$ cells (510 bp) is significantly narrower than that in WT cells (920 bp). Thus, the combined loss of HMGN1 and HMGN2 significantly altered the DNase I sensitivity of the MEFs. The newly formed sites in $Hmgn1^{-/-}n2^{-/-}$ MEFs were significantly narrower than the average sites seen in WT cells, suggesting a general decrease in DNA accessibility at chromatin regulatory regions.

Preferential loss of DHSs at enhancers in $Hmgn1^{-/-}n2^{-/-}$ MEFs.

Chromatin regulatory regions are marked not only by increased DNase I hypersensitivity but also by specific histone modifications such as H3K4me1, H3K27ac and H3K4me3, which mark enhancers, active enhancers, and promoters, respectively (Thurman et al. 2012; Calo and Wysocka 2013). Genome wide mapping of these histone marks in WT and $Hmgn1^{-/-}n2^{-/-}$ MEFs indicated that loss of both HMGN1 and HMGN2 did not affect the level of these 3 histone modifications (Fig. S4). However, alignment of the DHSs with these histone modifications reveals that loss of both HMGN1 and HMGN2 affected mainly the DHSs located in enhancer

regions. We detected 60,000 DHSs at enhancer regions of WT MEFs but only 23,000 DHSs at the $Hmgn1^{-/-}n2^{-/-}$ enhancers; thus, over 50 % of the DHSs detected at the WT enhancers were lost or significantly diminished in $Hmgn1^{-/-}n2^{-/-}$ MEFs (Fig. 3A and Fig. S5). Indeed, only 3% of the lost and 1% of the gained DHSs overlapped with H3K4me3, a marker for promoter; the great majority of DHSs that were either lost or gained overlapped with H3K4me1 and H3K27ac, histone marks for enhancer regions (Fig. 3B). The loss of DHSs at enhancer regions marked by H3K4me1 in $Hmgn1^{-/-}n2^{-/-}$ MEFs, but not in $Hmgn1^{-/-}$, or $Hmgn2^{-/-}$ MEFs lacking a single HMGN variant, is visualized by the heat map in Fig. 3C, and by the decreased normalized DHSs intensity overlapping the H3K4me1 or H3K27ac marks (Fig. 3D, E). The genomic snapshots of $Hmgn1^{-/-}n2^{-/-}$ cells shown in Fig.3G exemplify the unaltered profiles of H3K4me1, H3K4me3 and H3K27ac and the preferential loss of DHSs at sites overlapping with H3K4me1 and H3K27ac, but not at H3K4me3.

As a consequence of the significant loss of DHSs at enhancer regions, the DNA fragments at promoter regions, which are marked by H3K4me3, were disproportionally overrepresented in the sequenced libraries, resulting in a significant increase in the normalized intensity (reads per million) at H3K4me3 sites (Fig. 3F), thereby giving the false impression that in $Hmgn1^{-/-}n2^{-/-}$ MEFs the DNase I accessibility at these sites is increased. In fact, quantitative DNase I digestion analyses of regions overlapping with either H3K4me1 or H3K4me3 from the same gene indicates that both the promoter and the enhancer region in $Hmgn1^{-/-}n2^{-/-}$ MEFs were less digested than the same regions in WT MEFs (Fig. 4 A-C). In agreement with the genome wide analyses, the effects at H3K4me1 sites are significantly bigger than at H3K4me3 sites. The differences are most obvious when comparing the % of digested chromatin in WT to that in $Hmgn1^{-/-}n2^{-/-}$ MEFs, at the same DNase I concentration. For example, at the H3K4me1 site in the

9

Wrb locus, 2000 units/ml DNase I digested 74.6% of the site in WT cells but only 13.3% of the sites in *Hmgn1*$^{-/-}$*n2*$^{-/-}$ cells, a 5.6 fold difference. But at the H3K4me3 site, loss of HMGN1 and HMGN2 reduced the % of chromatin digested by only 1.5 fold, from 87% to 60.2% (Fig. 4A)

Taken together, our results reveal that loss of both HMGN1 and HMGN2 alters the DNase I hypersensitivity in chromatin globally, and that these affects are more pronounced at enhancer regions marked by H3K4me1-modified histones, than at promoter regions marked by H3K4me3 histones.

Altered nucleosome organization at promoters of *Hmgn1*$^{-/-}$*n2*$^{-/-}$ MEFs.

DNase I hypersensitivity at regulatory sites results from perturbed nucleosome occupancy. The nucleosome ladders originating during the MNase digestion of WT and *Hmgn1*$^{-/-}$*n2*$^{-/-}$ cells were indistinguishable, indicating that loss of HMGNs does not have significant effects on global chromatin compaction (Fig. 4D). To test the effects of HMGN variants on nucleosome occupancy at regulatory sites, we mapped the genomic nucleosome positions in WT and *Hmgn1*$^{-/-}$*n2*$^{-/-}$ MEFs, by deep sequencing of mononucleosomal DNA purified from either limited, or extensive micrococcal nuclease (MNase) digestions, when either only ~5%, or more than ~80% of the chromatin is converted to mononucleosomes, respectively, (Fig. 4D). The limited digests are enriched in DNA fragments originating from the nucleosomes located in the decondensed, regulatory regions of chromatin. The linker regions of these nucleosomes are more accessible to the enzymes and therefore during the digestions these nucleosomes are released first and then further digested; consequently, the DNA from regulatory regions is disproportionally underrepresented in extensive MNase digests.

10

Deep sequencing of DNA recovered from extensive digests of WT and $Hmgn1^{-/-}n2^{-/-}$ MEFs revealed a "nucleosome free region" at the TSS (Fig. 4E, top), as was seen in other cells (Jiang and Pugh 2009). In contrast, the DNA of the nucleosomes from the limited MNase digestions clearly reveals the presence of a nucleosome positioned at the TSS, in the "nucleosome free regions" seen in extensive digests. Significantly, in the limited digests, the occupancy of nucleosomes at the TSS of $Hmgn1^{-/-}n2^{-/-}$ MEFs was higher than in WT MEFs (Fig. 4E, bottom) indicating that loss of HMGNs enhances the stability of the nucleosomes that are located at regulatory sites, a finding that is in full agreement with the reduced DNase I sensitivity of these cells.

Altered stress-induced gene expression in $Hmgn1^{-/-}n2^{-/-}$ MEFs.

Since changes in DNase I hypersensitivity could affect gene expression, we sequenced the RNA isolated from exponentially growing MEFs and tested whether loss of HMGNs changed the cellular transcriptome. We find that loss of HMGN1, HMGN2, or both these variants, altered the expression of 22, 49 and 77 genes, respectively (Fig. S6, Table S3). GO analysis failed to reveal specific pathways affected by these genes, reinforcing previous findings that unlike transcription factors, HMGNs do not target specific genes and are not major regulators of specific gene expression.

As an additional test of the consequences of the altered DHSs landscape on gene expression, we measured the kinetics of the transcriptional responses known to involve rapid changes in chromatin. To this end we measured the transcriptional response to stress induced either by treatment with the protein synthesis inhibitor anisomycin (Mahadevan et al. 1991) or by exposure to heat shock (Corey et al. 2003), treatments that induce the expression of specific genes. We exposed WT and $Hmgn1^{-/-}n2^{-/-}$ MEFs to anisomycin and quantified the transcriptional

11

response of 44 "immediate-early" genes (Fig. 5A, Table S4) known to be induced by stress (Tullai et al. 2007). Of the 44 genes tested, 22 showed significant differences in the induction kinetics with 18 of these genes induced faster, and 4 genes induced slower in $Hmgn1^{-/-}n2^{-/-}$ MEFs, as exemplified by the induction kinetics of $Ccl2$ and $Il6$ genes (Fig. 5B,C). We also calculated the difference in induction ratio between the 2 biological replicates of WT and $Hmgn1^{-/-}n2^{-/-}$ MEFs, and compared them with the differences seen between $Hmgn1^{-/-}n2^{-/-}$ and WT MEFs (Fig. S7). The observed significant differences in the induction kinetics between $Hmgn1^{-/-}n2^{-/-}$ and WT cells were eliminated between the replicates of the same genotype, indicating that the differences are s due to the loss of HMGNs and not to variance between biological replicates. The genes with altered expression showed loss of DHSs in $Hmgn1^{-/-}n2^{-/-}$ MEFs, especially at enhancer sites marked by H3K4me1, as shown by the example in Fig 5D. Likewise, the heat shock-induced transcriptional activation of $Hspa1a$ and $Hspa1b$, known to be accompanied by a rapid chromatin re-structuring, was slower in $Hmgn1^{-/-}n2^{-/-}$ MEFs (Fig. 5E). Loss of HMGN1 and HMGN2 leads to significant changes in the DHSs at the promoters of both $Hspa1a$ and $Hspa1b$ genes (Fig. 5F).

Altered phenotypes in $Hmgn1^{-/-}n2^{-/-}$ mice.

In the biological context of an entire organism, we compared the transcription profile in brain, liver, spleen and thymus in each of the three $Hmgn^{-/-}$ lines, to the corresponding wild type controls. Loss of HMGN1, HMGN2, or both these variants, affected the expression of a limited number of genes in each tissue, with similar number of genes up and down regulated. The number of genes changed in $Hmgn2^{-/-}$ tissues was comparable to the changes in tissues from $Hmgn1^{-/-}n2^{-/-}$ mice, both of which were higher than the number of genes changed in $Hmgn1^{-/-}$ tissues (Fig. 6 A-D). There was very little overlap between the genes affected in the various mouse lines (Fig. 6 E-H) or between the four tissues taken from a mouse line (Fig. 6 I-K)

12

reinforcing previous findings indicating tissue specific and HMGN variant specific effects on transcription (Kugler et al. 2013).

In addition to examining the genes with significant changes in gene expression, we also analyzed the effect of HMGN loss on cellular transcription pathways, disregarding the magnitude of change in the expression levels of individual genes. In this analysis, we averaged the expression level of the four WT mice, and compared this average to each of their four genetically altered littermates. Running one-sample t-test on fold changes of genes, we identified several pathways in which the expression of a significant number of genes was affected, in each of the four mice, in the three mouse lines examined (Table S5). The significant number of genes affected in a particular pathway raises the possibility that the cumulative effects of small changes in the transcription of several genes may be functionally relevant and lead to altered phenotypes.

Phenotypic screening of 15 male and 15 female *Hmgn* mutant mice and their WT controls, a total of 30 mice for each genotype, were performed at the German Mouse Clinic using a standard battery of tests (Fuchs et al. 2009; Gailus-Durner et al. 2009). In these tests, *Hmgn1$^{-/-}$n2$^{-/-}$* mice showed significantly more altered phenotypes than either *Hmgn1$^{-/-}$* or *Hmgn2$^{-/-}$* mice (Table 1, and supplement to Table 1). Metabolic screening of *Hmgn1$^{-/-}$n2$^{-/-}$* mice indicated increased food intake but decreased body mass, perhaps linked to increased energy expenditure. Likewise, clinical chemistry analyses of these mice revealed changes in the levels albumin and alpha amylase activity, as well as changes in triglyceride, cholesterol, and insulin levels of mice lacking both HMGN variants that were not detected in mice lacking a single variant. Additional noticeable differences were detected as changes in the distribution of leukocyte subpopulations in the blood of *Hmgn1$^{-/-}$n2$^{-/-}$* mice which showed higher frequencies of T, NK and NKT cells, altered CD4+ to CD8+ ratios in T cells, and changes in the distribution of the cells in the NK and

B cell compartment. Furthermore, $Hmgn1^{-/-}n2^{-/-}$ mice showed not only a reduced corneal thickness which was also seen in $Hmgn1^{-/-}$ mice (Birger et al. 2006), but also significantly enlarged eye axial lengths and increased number of the fundic main blood vessels; phenotypes which were not observed in either $Hmgn1^{-/-}$ or $Hmgn2^{-/-}$ eyes. Thus, $Hmgn1^{-/-}n2^{-/-}$ mice show changes in eye morphology that were not seen in mice lacking a single HMGN variant, most likely because both variants are strongly expressed in the eye (Lucey et al. 2008). Thus, the phenotypic analyses indicate that loss of both HMGN1 and HMGN2 lead to more detectable phenotypes then loss of only HMGN1 or HMGN2, a finding that is in general agreement the compensatory binding of HMGN variants to chromatin and with the more severe changes in the DHSs landscape of $Hmgn1^{-/-}n2^{-/-}$ mice.

DISCUSSION

Elucidation of the factors that affect the establishment and maintenance of the DHSs sites may provide insights into the mechanisms whereby chromatin dynamics affect the cellular phenotype. We now show that HMGN variants modulate the DHSs landscape in the chromatin of MEFs. The combined loss of both HMGN1 and HMGN2 remodels the DHS landscape of MEFs in three measurable ways: part of the DHSs are lost, new DHSs are formed, and all the DHSs are less prominent, as measured by the number of nucleotides encompassed acoss a site. The overall effect of loss of the HMGN variants is a decrease in the DNase I hypersensitivity. Given the ubiquitous presence of HMGN proteins in vertebrate cells, it is likely that HMGN variants will similarly affect the organization of chromatin regulatory sites in other cells.

Most of the prominent DHSs are located at promoters and enhancers, regulatory chromatin sites that are also marked by specific modifications in the N-terminal tail of histone

14

H3. Although loss of HMGNs did not affect the levels of these histone modifications, it affected the DNase I hypersensitivity at enhancers to a significantly larger extent than at promoters. Over 70% of the DHSs sites that changed in $Hmgn1^{-/-}n2^{-/-}$ MEFS localized to enhancer regions; there were twice as many DHSs lost as newly formed. Furthermore, all the DHSs of $Hmgn1^{-/-}n2^{-/-}$ MEFS, regardless whether lost, gained or shared, were narrower than the sites of WT MEF. For these experiments, the quality and depth of all our sequencing samples are sufficiently high (Supplemental Table S1). Although there are known limitations in peak calling algorithms, we think that it is an indispensable initial screening in identifying potential regions of interest. Additionally, we included an aggregate DHS accessibility plot (Fig. S5).

DNase I digestion is a continuous enzymatic process in which most of the chromatin will eventually be reduces to very small fragments; the DHSs landscape provides a snapshot of an early kinetic point in the digestion. Therefore, the disappearance of a site does not necessarily mean that the site is fully lost; it means that the site is less accessible to the enzyme, as we demonstrate in the quantitative DNase I digestion of promoter and enhancer regions of the same gene (Fig. 4A). Significantly, although loss of HMGNs leads to a global reduction in DNase I hypersensitivity, we also find that $Hmgn1^{-/-}n2^{-/-}$ MEFs contain new DHSs that were not detected in WT cells, an indication that these regions became more accessible to the enzyme. Thus, loss of HMGNs remodels the DHSs landscape of the cells: while most of the regulatory sites become less sensitive to DNase I, new sites which are more accessible to digestion are formed.

Enhancer regions are the most variable and rapidly evolving class of chromatin regulatory sites and show a cell type specific pattern that is altered during differentiation and development (Heintzman et al. 2009; Thurman et al. 2012; Calo and Wysocka 2013; Villar et al. 2015). Our finding that HMGN variants preferentially remodel DHSs at enhancers, the most

15

malleable and dynamic part of the genome, raises the possibility that these proteins help optimize chromatin remodeling during evolution, differentiation, or in response to stimuli that evoke changes in gene expression.

HMGNs could remodel the DHSs landscape by altering the action of factors known to establish and modulate DNase I hypersensitivity. The levels of H3K4me1, H3K4me3, and H3K27ac modifications were not altered in $Hmgn1^{-/-}n2^{-/-}$ MEFS indicating that the HMGN-mediated chromatin remodeling is not due to changes in these histone modifications. HMGNs could modulate the ability of regulatory factors to interact with chromatin, as was shown for PCNA (Postnikov et al. 2012), or the action of ATP-dependent nucleosome remodeling factors (Rattner et al. 2009) which play a role in the organization of local chromatin structures. An additional important mechanism potentially contributing to the HMGN mediated changes in DHSs could involve alterations in the interaction of the linker histone H1 with chromatin. Linker H1 variants, the most abundant chromatin binding proteins, have been shown to stabilize chromatin compaction and decrease chromatin accessibility (Bustin et al. 2005; Woodcock et al. 2006; Li et al. 2012). The interaction of HMGNs with nucleosome is known to reduce the binding of H1 to chromatin, both *in vivo* and *in vitro* (Ding et al. 1997; Catez et al. 2002; Catez et al. 2006; Rochman et al. 2009). Loss of HMGNs could enhance H1 binding, thereby reducing the accessibility of the DNA at chromatin regulatory sites to DNase I digestion. Most likely, the cumulative effects of changes in several factors that affect chromatin accessibility and remodeling lead to changes in nucleosome occupancy at regulatory sites, as we detected in the promoters of $Hmgn1^{-/-}n2^{-/-}$ MEFs (Fig. 4D). Thus, we suggest that HMGNs play a role in maintaining the DHSs landscape by modulating the interaction of regulatory factors and architectural proteins with chromatin.

Global changes in gene expression occurring during development and differentiation, or in response to alteration in transcription factor availability, are often associated with changes in the DHSs landscape (Voss and Hager 2014). Surprisingly, in $Hmgn1^{-/-}n2^{-/-}$ MEFs growing at optimal conditions, the changes in DHSs were accompanied with only minor changes in gene expression, perhaps because loss of the HMGN variants did not alter the histone marks at regulatory sites and did not detectably change the level of chromatin regulators. Thus, in the absence of additional changes or stress, an altered DHSs landscape does not necessarily lead to significant changes in transcription. Indeed, the stress induced transcriptional response in $Hmgn1^{-/-}n2^{-/-}$ MEFs was different from that of WT MEFs, supporting the suggestion that the presence of HMGNs facilitates chromatin remodeling. We note however that these changes were not very large and in most cases the loss of HMGNs increased the rate of induction of the immediate early genes, an unexpected result. An obvious possible explanation is that loss of DHSs decreased the binding of a negative regulator to a site that affects the induction of immediate gene expression. In addition, it is known that the induction of immediate early gene expression is associated with, and affected by, phosphorylation of H3S10, and that loss of HMGN1 enhances the rate of this phosphorylation (Lim et al. 2005). The results reinforce the general notion that by itself, the presence of DNase I site cannot predict the gene expression levels.

Transcriptional profiling of tissues from genetically altered HMGN mice showed few significant differences between the four tissues taken from mice lacking HMGN variants and their wild type littermates. Yet, compared to WT littermates, the phenotype of $Hmgn1^{-/-}n2^{-/-}$ mice was more significantly affected than that of mice lacking a single variant. Most likely, the phenotypes result from the accumulated changes in the transcription level of numerous genes

17

which at the individual gene are not highly significant, as suggested by the small but numerous changes in the expression of genes in several distinct pathways.

Considering the interaction of HMGN variants with chromatin, our ChIP analyses demonstrating that loss of one variant increases the nucleosome binding of the remaining variant provide direct evidence for an interplay among HMGNs, as was suggested by fluorescence analyses of living cells (Catez et al. 2002). The interactions among HMGN variants are functionally relevant since distinct changes in the DHSs landscape are seen when both variants are missing. However, the biological functions of the various HMGNs are not necessary identical; each HMGN variant forms unique complexes with nucleosomes (Postnikov et al. 1995) raising the possibility of variant-specific effects on the function of chromatin regulators thereby leading to variant specific contributions to an observed phenotype.

MATERIALS AND METHODS

Generation of *Hmgn1$^{-/-}$*, *Hmgn2$^{-/-}$* and *Hmgn1$^{-/-}$n2$^{-/-}$* knockout mice.

Hmgn1$^{-/-}$ mice, lacking exons 2-4 of the gene were previously described (Birger et al. 2003; Kugler et al. 2013). The targeting vector for generating the *Hmgn2$^{-/-}$* , lacking the entire gene, was constructed by a recombinogenic cloning strategy (Liu et al. 2003) with a murine bacterial artificial chromosome clone, RP23-31L13. The vector was constructed to remove the entire gene, encompassing exon 1-6 (Fig. S1A). A 16-kb fragment containing *Hmgn2* gene was retrieved from the bacterial artificial chromosome clone and inserted into the targeting vector PL253 by recombination in bacterial strain DY380. The neo gene with the phosphoglycerate kinase 1 promoter (pGK-neo) was employed as a positive selectable marker, and the pGK-thymidine kinase cassette was used as a negative selectable marker. The Frt-flanked pGK-neo

18

and the loxP sites for conditional deletion of *Hmgn2* were inserted as described in Fig. S1A.

Electroporation and selection were performed by using the v6.4 embryonic stem (ES) cell line.

DNAs derived by G418/1,2'-deoxy-2'-fluoro-1-β-D-arabinofuranosly-5-iodo-uracil-resistant ES

cell clones were screened by diagnostic *Bam*HI restriction enzyme digestion using the 5' probes

external to the targeting vector sequence. Two independent ES cell clones targeted to *Hmgn2*

were injected into C57BL/6 blastocysts and generated chimeras that transmitted the mutated

allele to the progeny. The neomycin resistance (neo) and the *Hmgn2* gene were removed by

crossing with beta actin Cre mice. The mice containing the targeted allele were backcrossed into

the C57BL/6 background for at least five generations. To generate $Hmgn1^{-/-}n2^{-/-}$ mice, the

$Hmgn2^{-/-}$ mice were crossed with $Hmgn1^{-/-}$. All mice were bred in a specific pathogen-free

facility with food and water *ad libitium*. At the GMC, mice were maintained according to the

GMC housing conditions and German laws. All tests performed at the GMC were approved by

the responsible authority of district government of Upper Bavaria, Germany.

Phenotype screening of 15 male and 15 female *Hmgn* mutant mice and their age matched

WT littermates or corresponding WT controls for the $Hmgn1^{-/-}n2^{-/-}$ knockout mice, a total of 30

mutant and 30 control mice for each mouse line, were performed at the German Mouse Clinic

using a standard battery of tests (Gailus-Durner et al. 2005; Fuchs et al. 2009; Gailus-Durner et

al. 2009; Fuchs et al. 2011) The detailed phenotypic analysis of the mice is described in

Supplemental Data. A complete description of the methods can be found at the German Mouse

Clinic website (www.mouseclinic.de).

Preparation of primary mouse embryonic fibroblasts (MEFs) and neuroprogenitors.

MEFs were prepared from E13.5 Embryos. After removal of the head and viscera, the embryos were digested in 0.25% trypsin at 37°C, with gentle pipetting for 30 min. The dissociated fibroblasts were allowed to settle and then cultured in 150 cm plates in DMEM (Corning) with 10% FBS (Life Technologies) under 5% CO_2 at 37°C. All experiments were done with MEFs at passage 3. For each genotype, 2 independent MEF clones (biological replicates) were used in every experiment, including DNase-seq, and MNase-seq. Neuroprogenitors were prepared from embryonic stem cells differentiated along the neural lineage using a mouse dopaminergic neuron differentiation kit (R&D systems, Minneapolis, MN) as described (Deng et al. 2013).

Western blotting and Immunostaining

Rabbit affinity pure polyclonal anti-mouse HMGN1, anti-human HMGN2 and anti-calf Histone H1 antibodies were generated in our laboratory (Birger et al. 2003). HRP-conjugated secondary antibodies for Western Blots were from Pierce. Fluorescence secondary antibody was AlexaFluor488-donkey-anti-rabbit IgG (Invitrogen). For Western blots, whole cell lysates were prepared in 1×SDS PAGE sample buffer (Bio-Rad) supplemented with protease inhibitors (Roche Applied Science). The samples were fractionated on 15% pre-cast Criterion gels, transferred by semi-dry method to PVDF membrane, blocked with non-fat milk in TBST and probed with antibodies. Chemiluminiscent detection using ECL Plus has been performed according to Amersham recommendations.

For immunostaining, 5 μm paraffin embedded liver sections were prepared from 8-weeks old *Hmgn2*$^{+/+}$ and *Hmgn2*$^{-/-}$ mice. Immunofluorescence staining was performed using anti-human HMGN2 antibody as previously described (Cherukuri et al. 2008). The images were

20

taken using Nikon Eclipse E800 fluorescence microscope and processed using NIS-Elements software (Nikon).

ChIP-seq

MEFs were crosslinked directly in culture medium with 1% formaldehyde solution for 10 minutes at room temperature. Chromatin was fragmented to 200-300 bp by 15 cycles of sonication (30s on/30s off) (Bioruptor). Chromatin from 2×10^7 cells and 10 µg antibodies against HMGN1, HMGN2, H3K4me1 (Abcam, ab8895), H3K4me3 (Abcam, ab8580) and H3K27ac (Abcam, ab4729) were used for each ChIP experiment. Sequencing libraries were prepared using Illumina TruSeq ChIP Sample Prep Kit with compatible indexed adaptors according to manufacturer's instruction. Equal amounts of 4-6 indexed library samples were pooled for cluster generation and sequenced on Illumina HiSeq 2000 system with 2×100 bp paired-end reads.

Genome-wide mapping of DNase I hypersensitivity sites

For preparation of nuclei, MEFs were incubated on ice for 10 minutes in Buffer A (0.15M Tris-HCl pH8.0, 15mM NaCl, 60mM KCl, 1mMEDTA, 0.5mMEGTA) containing 0.03% IGEPAL (Sigma), 1mM EDTA, 0.5mM EGTA, 0.5mM spermidine and protease inhibitor (Roche Applied Science). DNase I digestion was carried out by incubation of 2×10^7 nuclei with 2000 U/ml DNase I (Roche Applied Science) at 37°C for 3 minutes. After treatment by RNase A and proteinase K, DNA was recovered by phenol / chloroform extraction. DNA fragments with size 150-500 bp were isolated by 9% sucrose gradient centrifugation. Libraries construction and sequencing were performed as described above for ChIP-seq samples.. DNase I accessibility assays were performed to validate the sequencing results. Kinetic DNase I digestion assays were

done using 1000, 2000 or 3000 U/ml DNase I. The digested DNA was precipitated and equal amount of DNA was analyzed by quantitative real-time PCR. Primer information is presented in Table S2.

Genome-wide nucleosome positioning assay

Mono-nucleosomal DNA from MEFs was isolated by micrococcal nuclease digestion using EZ Nucleosomal DNA Prep Kit (Zymo Research) according to the manufacturer's instruction. In brief, nuclei were isolated from trypsinized cells by incubation on ice for 5 minutes in Nuclei Prep Buffer. 1.5×10^{6} nuclei were then digested by 0.05 - 0.5 units of micrococcal nuclease in 100 μL MN Digestion Buffer at room temperature for 10 minutes. DNA was purified from the nuclear digests using the columns supplied with the kit and fractionated on 2% agrose-gels . Mono-nucleosomal DNA was purified from the gels using a Qiagen gel extraction kit and processed for libraries construction and deep sequencing as described above for ChIP-seq.

Gene expression analysis

Transcription analysis in MEFs were performed by RNA-sequencing. Total RNA was isolated by RNeasy Mini Kit (Qiagen) followed by "on-column" DNase I treatment. mRNA-seq libraries were prepared from 1 μg of total RNA using the Illumina TruSeq RNA Sample Preparation Kit, following the manufacturer's instructions. Libraries were sequenced on the Illumina HiSeq 2000 with 2×100 bp paired-end reads. The data analysis was performed using the RNA-seq pipeline in Partek Genome Suite. A gene was considered expressed if reads per kilobase of transcript model per million mapped reads (RPKM) was ≥ 1.0. |Fold Change| ≥ 1.5 with P-value < 0.05 was considered significantly differentially expressed between two genotypes.

For analysis of gene expression in mouse tissues and identification of differentially-expressed genes between wild type and mutant mice, amplified cRNA was hybridized to MouseRef-8 Version 2 Expression BeadChips (Illumina, San Diego) and after a 16-h incubation, staining and scanning were done according to the Illumina expression protocol. To identify differentially regulated genes, we used the mattest function of the MATLAB package. A permutation method (Storey and Tibshirani 2003) has been employed to address the small sample size and 5,000 permutations have been performed using the mattest function. Differently-expressed genes were selected using a uniform cutoff - p value < 0.05 and fold change > 1.5 - in all cases.

Bioinformatic DNase-seq, ChIP-seq and MNase-seq analyses

Unfiltered sequencing reads (from DNase-seq, ChIP-seq, or MNase-seq) were aligned to the mouse reference genome (NCBI build 37, mm9) using Bowtie (Langmead et al. 2009). Up to 2 mismatches was allowed for each aligned read. Only uniquely aligned reads were collected for further analysis. The information of the quality and depth of all the sequencing samples are in Supplemental Table S1.

DNase-seq and ChIP-seq peaks were identified using SICER (Zang et al. 2009) with the following parameters: effective genome size, 0.875 (87.5% of the mouse genome is mapped by 100-bp reads); window size, 50 bp; gap size, 50 bp. Calculation of coverage and identification of overlapping regions were performed with the "chipseq" and "GenomicRanges" packages in BioConductor (Gentleman et al. 2004).

For normalization, the calculation of coverage at any regions and the comparisons between different data sets were preceded by library size normalization. Control subtraction was

23

carried out in the following way: coverage (exp)/N1 – coverage (control)/N2, in which "exp" is

the data set (in .bam format) to be examined, N1 is the library size of the experimental data

("exp"), and N2 is the library size of the control. In this study, input sequences (DNA sequences

after sonication only without immunoprecipitation) were used as a control for all histone

modification ChIP-seq data. The function coverage that calculates genome coverage from .bam

files is from the "chipseq" package in BioConductor.

Specifically, in analyzing MNase-seq data, since the reads are from the ends of the

mononucleosome particle, to best visualize the nucleosome positions, all the reads were shifted

to the middle of the corresponding nucleosome core. The average sizes of mononucleosome

fragments purified from a 2% agarose gel were determined by Bioanalyzer (Agilent).

Immediate early gene induction

WT and *Hmgn1^-/-^n2^-/-^* MEFs were grown in 1×DMEM (#10-013-CV, Corning)

supplemented with 10% fetal calf serum (#16000-044, Life Technologies). After reaching 60%

confluence, the cells were stimulated for the indicated times with 50 ng/ml anisomycin (#A9789,

Sigma-Aldrich). Next, the cells were scraped, and washed with saline. Total RNA was extracted

with TRIzol reagent (#15596-026, Invitrogen), followed by purification using RNeasy Plus Mini

kit (#74134, Qiagen). Transcription levels of 42 selected genes (Suplemental Table S4) were

determined by NanoString Expression Analysis, using custom-made nCounter® Gene

Expression CodeSets (NanoString Technologies). The hybridization mix containing 10µl

Reporter CodeSet, 10µl hybridization buffer, 5µl(100ng) RNA and 5µl Capture ProbeSet were

incubated at 65°C for at least 12 hours and immediately post-hybridized in an nCounter Prep-

station ((NanoString Technologies). The data were analyzed with nSlover Analysis Software

24

version 1.1. The expression levels of the 42-immediate early genes were normalized to *Gapdh*, *Gusb,* and *Pgk1*. The induction ratio for each gene at any time was calculated by dividing the fold induction of the gene in WT by that of *Hmgn1$^{-/-}$n2$^{-/-}$* . The Log2 of the ratios were subjected to hierarchical clustering algorithm of self-organizing heat maps (GeneSpring GX version 12.6, Agilent Technologies). All analyses were done on two biological replicates.

Heat Shock

Primary mouse WT and *Hmgn1$^{-/-}$ n2$^{-/-}$* embryonic fibroblasts were subjected to heat shock at 42°C for the times indicated. RNA was isolated immediately with TRIzol reagent (#15596-026, Invitrogen), following by purification using RNeasy Plus Mini kit (#74134, Qiagen). Quantitative real-time RT-PCR analysis was done using two primer pairs per gene and two biological replicates using SYBR Green RT-PCR reagent kits (#4309155, Applied Biosystem). ΔCt values were determined by subtracting the Ct value of PCR reaction obtained using of *Hspa1a* and *Hspa1b* genes from that of control sets of primers. Expression of *Hspa1a* and *Hspa1b* was calculated as $2^{-\Delta\Delta Ct}$ value for each time point and each genotype, assigning the expression of *Hspa1a* and *Hspa1b* at 0 min as 1 and calculating fold induction as a ratio to the expression at 0 min.

Functional analysis of expression profiles

To predict the impact of HMGN knock-outs on gene expression and alteration of biological pathways (each being comprised of a group of the genes), we also adopted a computation approach based on genome-wide expression profiles as described before (Kugker et al, 2013).

Data access

The data from this study have been submitted to the NCBI Sequence Read Archive (SRA; http://www.ncbi.nlm.nih.gov/sra) under accession number SRS779760.

REFERENCES.

Bianchi ME, Agresti A. 2005. HMG proteins: dynamic players in gene regulation and differentiation. *Current opinion in genetics & development* **15**(5): 496-506.

Birger Y, Davis J, Furusawa T, Rand E, Piatigorsky J, Bustin M. 2006. A role for chromosomal protein HMGN1 in corneal maturation. *Differentiation* **74**(1): 19-29.

Birger Y, West KL, Postnikov YV, Lim JH, Furusawa T, Wagner JP, Laufer CS, Kraemer KH, Bustin M. 2003. Chromosomal protein HMGN1 enhances the rate of DNA repair in chromatin. *EMBO J* **22**(7): 1665-1675.

Boyle AP, Davis S, Shulha HP, Meltzer P, Margulies EH, Weng Z, Furey TS, Crawford GE. 2008. High-resolution mapping and characterization of open chromatin across the genome. *Cell* **132**(2): 311-322.

Bustin M. 1999. Regulation of DNA-dependent activities by the functional motifs of the high-mobility-group chromosomal proteins. *Molecular and cellular biology* **19**(8): 5237-5246.

Bustin M. 2001. Chromatin unfolding and activation by HMGN(*) chromosomal proteins. *Trends in biochemical sciences* **26**(7): 431-437.

Bustin M, Catez F, Lim JH. 2005. The dynamics of histone H1 function in chromatin. *Molecular cell* **17**(5): 617-620.

Calo E, Wysocka J. 2013. Modification of enhancer chromatin: what, how, and why? *Molecular cell* **49**(5): 825-837.

Catez F, Brown DT, Misteli T, Bustin M. 2002. Competition between histone H1 and HMGN proteins for chromatin binding sites. *EMBO Rep* **3**(8): 760-766.

Catez F, Ueda T, Bustin M. 2006. Determinants of histone H1 mobility and chromatin binding in living cells. *Nat Struct Mol Biol* **13**(4): 305-310.

Cherukuri S, Hock R, Ueda T, Catez F, Rochman M, Bustin M. 2008. Cell cycle-dependent binding of HMGN proteins to chromatin. *Mol Biol Cell* **19**(5): 1816-1824.

Corey LL, Weirich CS, Benjamin IJ, Kingston RE. 2003. Localized recruitment of a chromatin-remodeling activity by an activator in vivo drives transcriptional elongation. *Genes & development* **17**(11): 1392-1401.

Cuddapah S, Schones DE, Cui K, Roh TY, Barski A, Wei G, Rochman M, Bustin M, Zhao K. 2011. Genomic Profiling of HMGN1 Reveals an Association with Chromatin at Regulatory Regions. *Molecular and cellular biology* **31**(4): 700-709.

Deng T, Zhu ZI, Zhang S, Leng F, Cherukuri S, Hansen L, Marino-Ramirez L, Meshorer E, Landsman D, Bustin M. 2013. HMGN1 modulates nucleosome occupancy and DNase I hypersensitivity at the CpG island promoters of embryonic stem cells. *Molecular and cellular biology* **33**(16): 3377-3389.

Ding HF, Bustin M, Hansen U. 1997. Alleviation of histone H1-mediated transcriptional repression and chromatin compaction by the acidic activation region in chromosomal protein HMG-14. *Molecular and cellular biology* **17**(10): 5843-5855.

Erdel F, Rippe K. 2011. Chromatin remodelling in mammalian cells by ISWI-type complexes--where, when and why? *The FEBS journal* **278**(19): 3608-3618.

Fuchs H, Gailus-Durner V, Adler T, Aguilar-Pimentel JA, Becker L, Calzada-Wack J, Da Silva-Buttkus P, Neff F, Gotz A, Hans W et al. 2011. Mouse phenotyping. *Methods* **53**(2): 120-135.

Fuchs H, Gailus-Durner V, Adler T, Pimentel JA, Becker L, Bolle I, Brielmeier M, Calzada-Wack J, Dalke C, Ehrhardt N et al. 2009. The German Mouse Clinic: a platform for

systemic phenotype analysis of mouse models. *Current pharmaceutical biotechnology* **10**(2): 236-243.

Gailus-Durner V, Fuchs H, Adler T, Aguilar Pimentel A, Becker L, Bolle I, Calzada-Wack J, Dalke C, Ehrhardt N, Ferwagner B et al. 2009. Systemic first-line phenotyping. *Methods Mol Biol* **530**: 463-509.

Gailus-Durner V, Fuchs H, Becker L, Bolle I, Brielmeier M, Calzada-Wack J, Elvert R, Ehrhardt N, Dalke C, Franz TJ et al. 2005. Introducing the German Mouse Clinic: open access platform for standardized phenotyping. *Nature methods* **2**(6): 403-404.

Gentleman RC, Carey VJ, Bates DM, Bolstad B, Dettling M, Dudoit S, Ellis B, Gautier L, Ge Y, Gentry J et al. 2004. Bioconductor: open software development for computational biology and bioinformatics. *Genome biology* **5**(10): R80.

Gross DS, Garrard WT. 1988. Nuclease hypersensitive sites in chromatin. *Annual review of biochemistry* **57**: 159-197.

Heintzman ND, Hon GC, Hawkins RD, Kheradpour P, Stark A, Harp LF, Ye Z, Lee LK, Stuart RK, Ching CW et al. 2009. Histone modifications at human enhancers reflect global cell-type-specific gene expression. *Nature* **459**(7243): 108-112.

Jiang C, Pugh BF. 2009. A compiled and systematic reference map of nucleosome positions across the Saccharomyces cerevisiae genome. *Genome biology* **10**(10): R109.

Kugler JE, Horsch M, Huang D, Furusawa T, Rochman M, Garrett L, Becker L, Bohla A, Holter SM, Prehn C et al. 2013. High mobility group N proteins modulate the fidelity of the cellular transcriptional profile in a tissue- and variant-specific manner. *The Journal of biological chemistry* **288**(23): 16690-16703.

Langmead B, Trapnell C, Pop M, Salzberg SL. 2009. Ultrafast and memory-efficient alignment of short DNA sequences to the human genome. *Genome biology* **10**(3): R25.

Li JY, Patterson M, Mikkola HK, Lowry WE, Kurdistani SK. 2012. Dynamic distribution of linker histone H1.5 in cellular differentiation. *PLoS genetics* **8**(8): e1002879.

Lim JH, West KL, Rubinstein Y, Bergel M, Postnikov YV, Bustin M. 2005. Chromosomal protein HMGN1 enhances the acetylation of lysine 14 in histone H3. *EMBO J* **24**(17): 3038-3048.

Liu P, Jenkins NA, Copeland NG. 2003. A highly efficient recombineering-based method for generating conditional knockout mutations. *Genome Res* **13**(3): 476-484.

Lucey MM, Wang Y, Bustin M, Duncan MK. 2008. Differential expression of the HMGN family of chromatin proteins during ocular development. *Gene Expr Patterns* **8**(6): 433-437.

Mahadevan LC, Willis AC, Barratt MJ. 1991. Rapid histone H3 phosphorylation in response to growth factors, phorbol esters, okadaic acid, and protein synthesis inhibitors. *Cell* **65**(5): 775-783.

Mueller-Planitz F, Klinker H, Becker PB. 2013. Nucleosome sliding mechanisms: new twists in a looped history. *Nature structural & molecular biology* **20**(9): 1026-1032.

Narlikar GJ, Fan HY, Kingston RE. 2002. Cooperation between complexes that regulate chromatin structure and transcription. *Cell* **108**(4): 475-487.

Postnikov YV, Kurahashi T, Zhou M, Bustin M. 2012. The nucleosome binding protein HMGN1 interacts with PCNA and facilitates its binding to chromatin. *Molecular and cellular biology* **32**(10): 1844-1854.

28

Postnikov YV, Trieschmann L, Rickers A, Bustin M. 1995. Homodimers of chromosomal proteins HMG-14 and HMG-17 in nucleosome cores. *Journal of molecular biology* **252**(4): 423-432.

Rattner BP, Yusufzai T, Kadonaga JT. 2009. HMGN proteins act in opposition to ATP-dependent chromatin remodeling factors to restrict nucleosome mobility. *Molecular cell* **34**(5): 620-626.

Rochman M, Postnikov Y, Correll S, Malicet C, Wincovitch S, Karpova TS, McNally JG, Wu X, Bubunenko NA, Grigoryev S et al. 2009. The interaction of NSBP1/HMGN5 with nucleosomes in euchromatin counteracts linker histone-mediated chromatin compaction and modulates transcription. *Molecular cell* **35**(5): 642-656.

Stergachis AB, Neph S, Reynolds A, Humbert R, Miller B, Paige SL, Vernot B, Cheng JB, Thurman RE, Sandstrom R et al. 2013. Developmental fate and cellular maturity encoded in human regulatory DNA landscapes. *Cell* **154**(4): 888-903.

Storey JD, Tibshirani R. 2003. Statistical significance for genomewide studies. *Proceedings of the National Academy of Sciences of the United States of America* **100**(16): 9440-9445.

Swygert SG, Peterson CL. 2014. Chromatin dynamics: Interplay between remodeling enzymes and histone modifications. *Biochimica et biophysica acta* **1839**(8): 728-736.

Thurman RE, Rynes E, Humbert R, Vierstra J, Maurano MT, Haugen E, Sheffield NC, Stergachis AB, Wang H, Vernot B et al. 2012. The accessible chromatin landscape of the human genome. *Nature* **489**(7414): 75-82.

Tullai JW, Schaffer ME, Mullenbrock S, Sholder G, Kasif S, Cooper GM. 2007. Immediate-early and delayed primary response genes are distinct in function and genomic architecture. *The Journal of biological chemistry* **282**(33): 23981-23995.

Ueda T, Catez F, Gerlitz G, Bustin M. 2008. Delineation of the protein module that anchors HMGN proteins to nucleosomes in the chromatin of living cells. *Molecular and cellular biology* **28**(9): 2872-2883.

Villar D, Berthelot C, Aldridge S, Rayner TF, Lukk M, Pignatelli M, Park TJ, Deaville R, Erichsen JT, Jasinska AJ et al. 2015. Enhancer Evolution across 20 Mammalian Species. *Cell* **160**(3): 554-566.

Voss TC, Hager GL. 2014. Dynamic regulation of transcriptional states by chromatin and transcription factors. *Nature reviews Genetics* **15**(2): 69-81.

Wippo CJ, Israel L, Watanabe S, Hochheimer A, Peterson CL, Korber P. 2011. The RSC chromatin remodelling enzyme has a unique role in directing the accurate positioning of nucleosomes. *The EMBO journal* **30**(7): 1277-1288.

Woodcock CL, Skoultchi AI, Fan Y. 2006. Role of linker histone in chromatin structure and function: H1 stoichiometry and nucleosome repeat length. *Chromosome Res* **14**(1): 17-25.

Zang C, Schones DE, Zeng C, Cui K, Zhao K, Peng W. 2009. A clustering approach for identification of enriched domains from histone modification ChIP-seq data. *Bioinformatics* **25**(15): 1952-1958.

FIGURE LEGENDS.

Figure1. Compensatory binding of HMGN variants to NPs chromatin. (A) Scatter plot

showing correlation between HMGN2 binding and DNase I hypersensitivity at all DHSs.

Normalized coverage depths of both HMGN2 and hypersensitivity were calculated at all DHSs,

sorted by DHSs coverage depths , grouped into 50 data point bins, and averaged. R = Pearson

correlation coefficient. **(B)** Venn diagrams showing the overlap in the chromatin occupancy

between HMGN1 and HMGN2 in wild type (WT) NPs and the HMGN2 occupancy in *Hmgn1*^{-/-}

NPs. **(C)** Scatter plot showing colocalization of HMGN1 and HMGN2 in WT NPs. ChIP-seq

signals are normalized over each site, in reads per million (RPM). **(D-F)** Redistribution of

HMGN2 occupancy upon loss of HMGN1. Shown is the occupancy of HMGN2 in WT and

Hmgn1^{-/-} NPs at sites occupied by either HMGN1, HMGN2, or both of the variants in WT cells.

Note the shift in HMGN2 occupancy from HMGN2 unique sites to HMGN1 unique sites. **(G.)**

Genome-browser view of HMGN occupancy in WT and *Hmgn1*^{-/-} NPs. All the Y-axis span from

0 to 0.5 as indicated.

Figure2. Altered DHSs landscape in *Hmgn1*^{-/-}*n2*^{-/-} MEFs. (A) Quantitative analyses of the

chromatin immunoprecipitated from either WT, *Hmgn1*^{-/-} or *Hmgn2*^{-/-} MEFs with antibodies to

either HMGN1 or HMGN2. Note that loss of either HMGN1 or HMGN2 variant increased the

amount of chromatin precipitated by the remaining variant. * P< 0.001. **(B-D)**Venn diagrams

showing the overlap in the DHSs between WT and either *Hmgn1*^{-/-} , *Hmgn2*^{-/-} , or *Hmgn1*^{-/-}*n2*^{-/-}

MEFs. **(E-G)** Scatter plot showing similar intensity of DHSs in WT and *Hmgn1*^{-/-} or *Hmgn2*^{-/-},

but not in *Hmgn1*^{-/-}*n2*^{-/-} MEFs. DHS signals are normalized by library size and averaged over two

biological replicates over each site, in reads per million (RPM). **(H-J)** Reduced DHS width in

Hmgn1^{-/-}*n2*^{-/-} MEFs. In *Hmgn1*^{-/-}*n2*^{-/-} MEFs, the mean width of all DHSs is narrower (H)**,** the

30

width of DHSs sites lost is larger than that of DHSs gained (I), and the shared DHS are narrower

(J), as compared to WT MEFs. Bars show frequency and curves show density. (**K**) Genome

browser snapshot visualizes the lost or gained DHSs in *Hmgn1⁻/⁻n2⁻/⁻* MEFs. Two biological

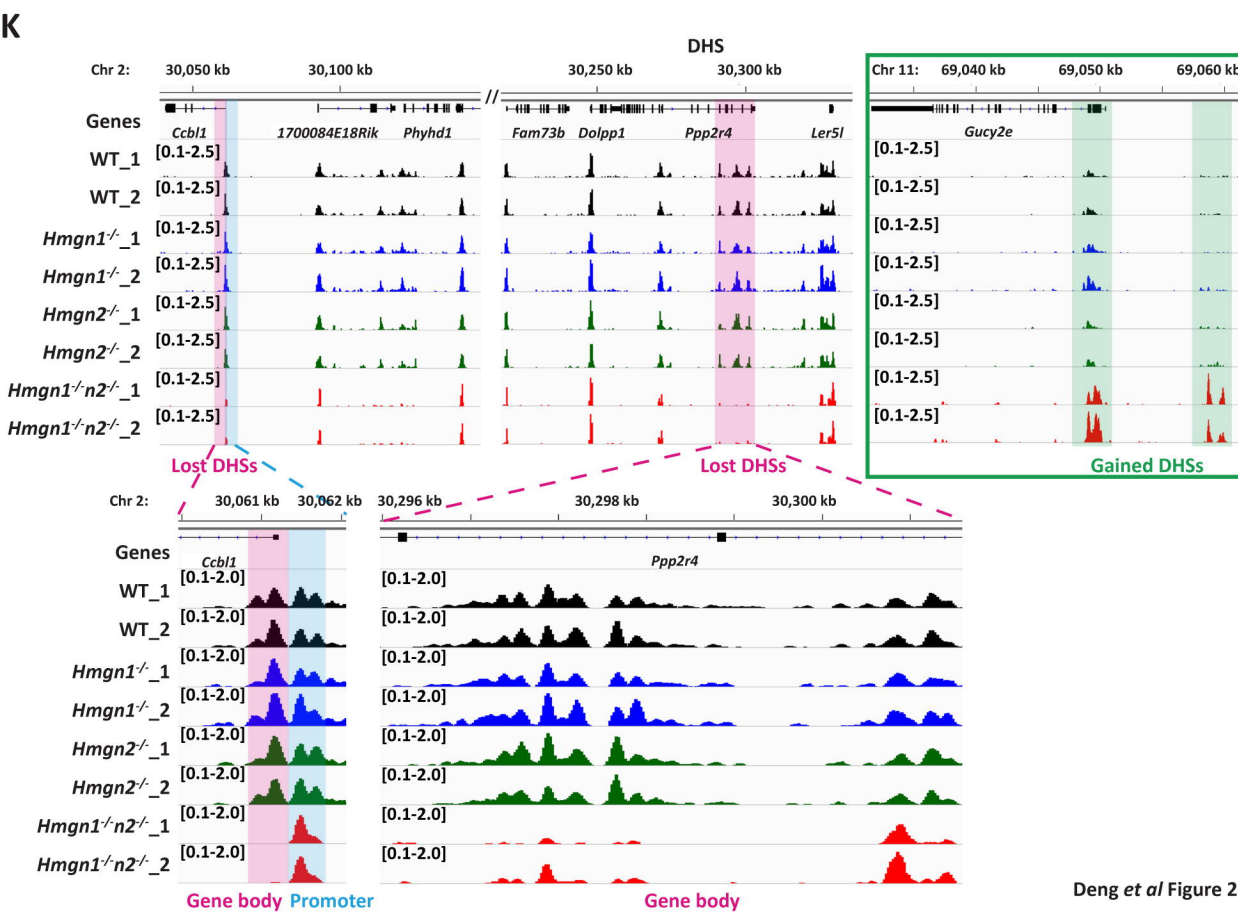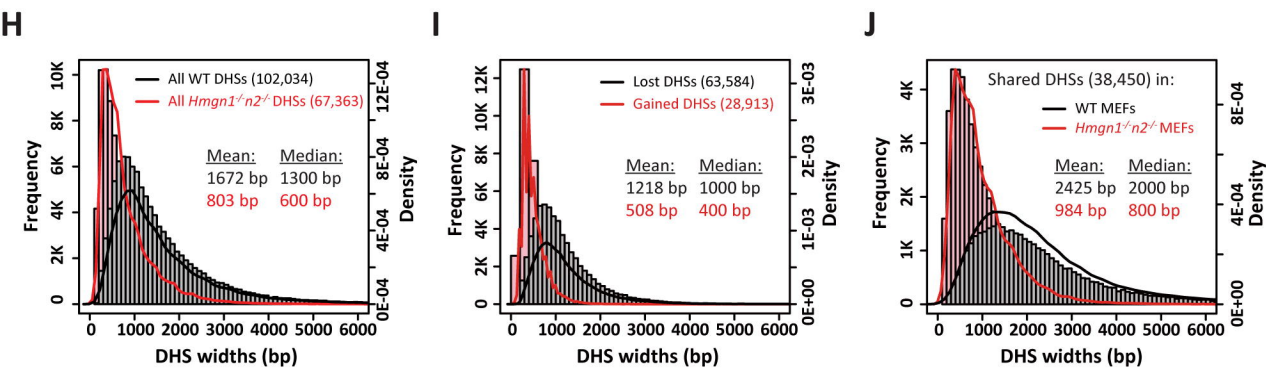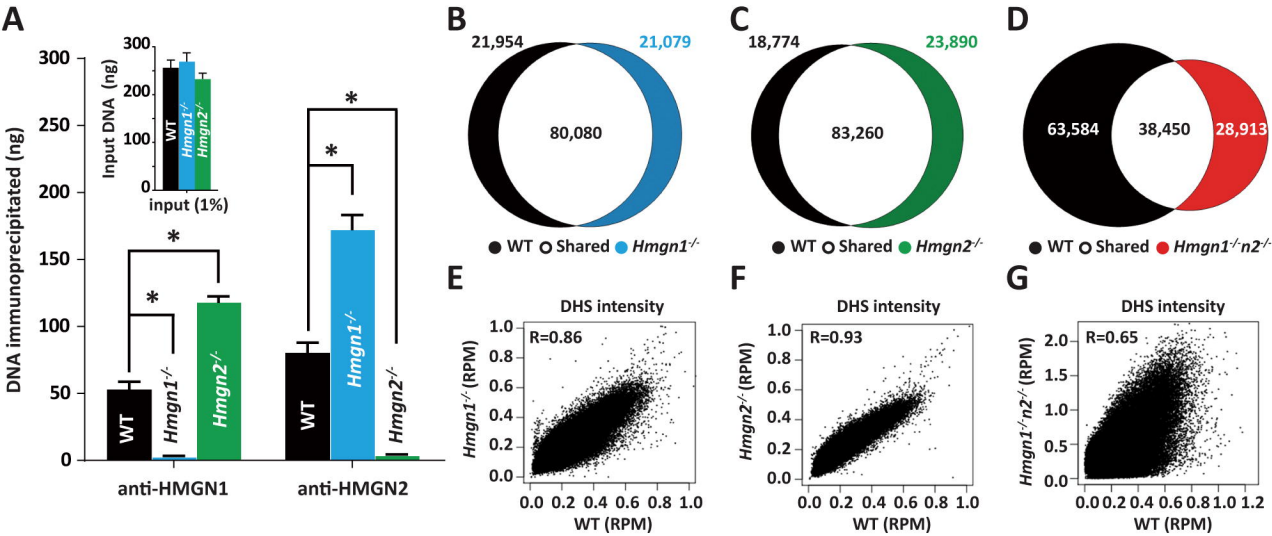replicates for each genotype are shown. Numbers in parenthesis indicate the scales of the Y axis.

Figure 3. Altered DHSs at *Hmgn1⁻/⁻n2⁻/⁻* enhancers. (**A**) Loss of DHSs at enhancers of

Hmgn1⁻/⁻n2⁻/⁻ MEFs. Shown is the DHSs distribution among annotated sequences in genome of

WT, *Hmgn1⁻/⁻* , *Hmgn2⁻/⁻* , and *Hmgn1⁻/⁻n2⁻/⁻* MEFs. (**B**) Changes in DHSs at regions overlapping

with enhancers (H3K4me1 or H3K27ac) but not promoters (H3K4me3). (**C**) Heat maps of DHS

intensities across all H3K4me1, not overlapping H3K4me3, peak regions (center-aligned),

visualizes the loss of DHSs at H3K4me1 regions in *Hmgn1⁻/⁻n2⁻/⁻* MEFs. (**D-F**) Normalized

average intensity of DHSs in WT and mutant MEFs, at indicated histone marks (**G**) Genomic

browser snapshot visualizing the preferential loss of DHSs at sites overlapping with H3K4me1

and H3K27ac in *Hmgn1⁻/⁻n2⁻/⁻* MEFs. Two biological replicates are shown for the DHSs maps.
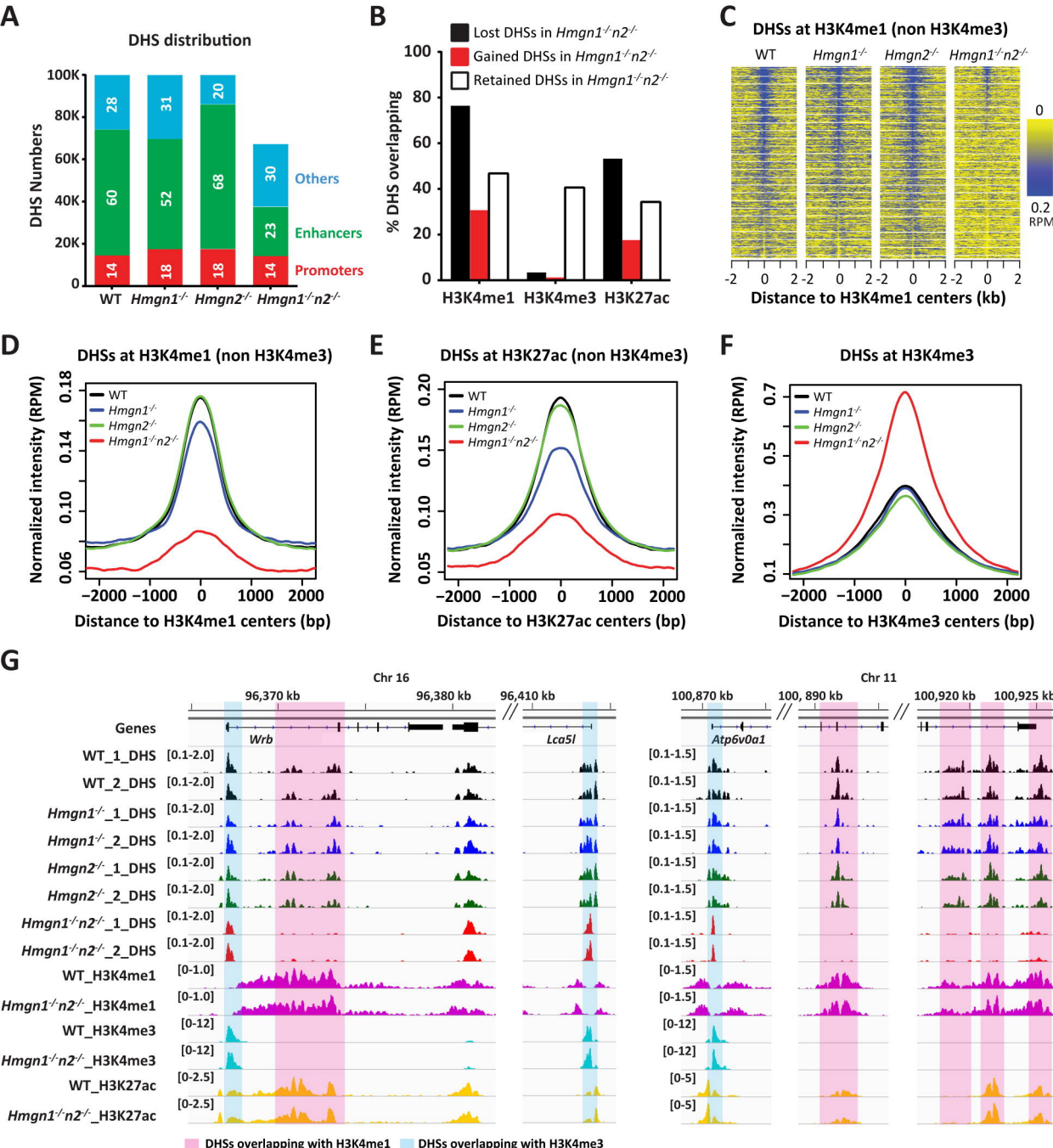
Numbers in parenthesis indicate the scales of the Y axis.

Figure 4. Altered nuclease sensitivity at regulatory chromatin sites of *Hmgn1⁻/⁻n2⁻/⁻* MEFs.
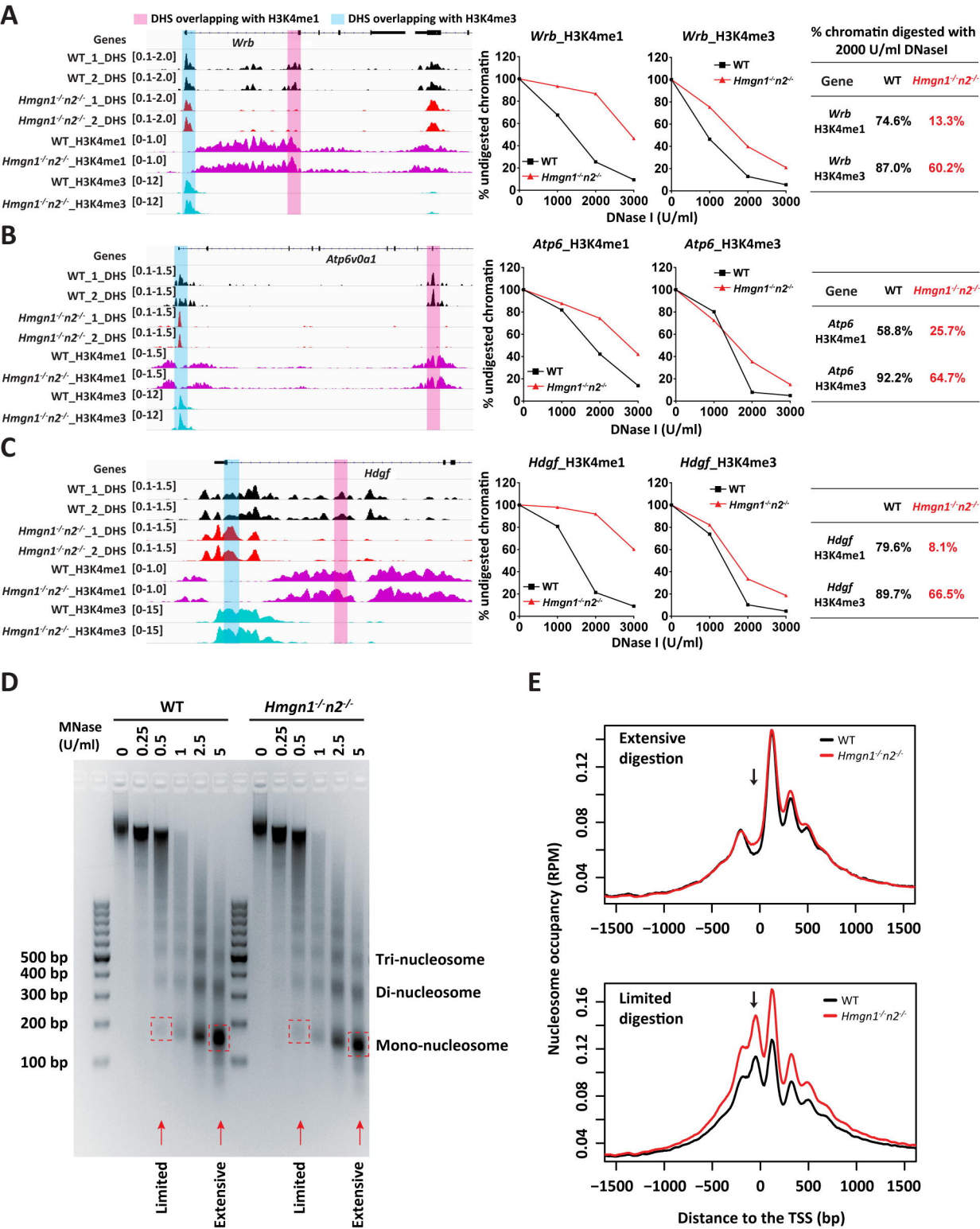
(**A-C**) Quantitative analysis of DNase I sensitivity at promoters and enhancers of 3 selected

genes. The extent of DNase I digestion at regions overlapping either H3K4me1 or H3K4me3

(pink or blue in genome browser), quantified by PCR amplification. Loss of HMGNs affected

regions overlapping with H3K4me1 more significantly than regions overlapping H3K4me3.

Numbers in parenthesis indicate the scales of the Y axis. (**D**) Loss of HMGN does not affect the

kinetics of MNase digestion. (**E**) Deep sequencing of nucleosome positons reveals enhanced

occupancy of unstable nucleosomes at the TSS of *Hmgn1⁻/⁻n2⁻/⁻* MEFs. Arrow points to the

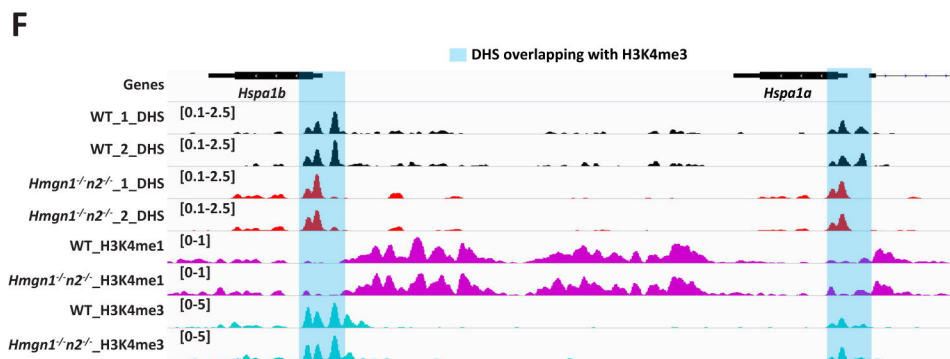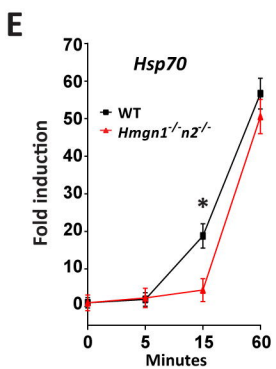presence of a nucleosome detectable at the TSS in limited, but not extensive digests.
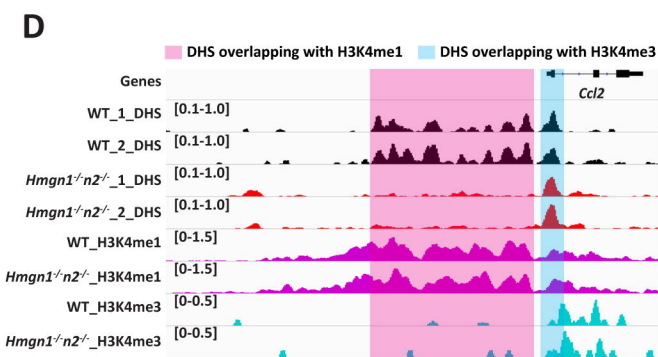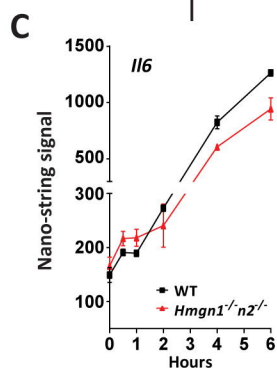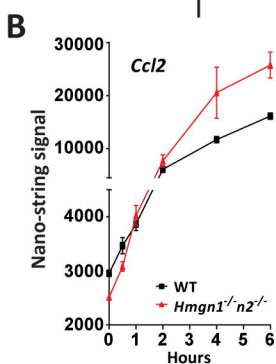
Figure 5. Altered immediate early (IE) gene expression in *Hmgn1$^{-/-}$n2$^{-/-}$* MEFs. (A) Heat map showing the induction fold ratios of IE genes in WT and *Hmgn1$^{-/-}$n2$^{-/-}$* MEFs. Boxes separate the genes that were s upregulated and down regulated from the unaffected genes. * P <0.05, Two biological replicates were analyzed. **(B, C)** Kinetics of Anisomycin induced expression of *Ccl2* and *Il6*. **(D)** Genome browser view of changes in DHSs at H3K4me1 and H3K4me3 sites 5 prime to the *Ccl2* gene. Numbers in parenthesis indicate the scales of the Y axis. **(E)** Altered induction of heat shock genes in *Hmgn1$^{-/-}$n2$^{-/-}$* MEFs. **(F)** Genome browser view of changes in DHSs at H3K4me1 and H3K4me3 sites near the *Hspa1a* and *Hspa1b* genes. Numbers in parenthesis indicate the scales of the Y axis.

Figure 6. Effect of HMGN loss on global gene expression in mouse tissues. (A-D). Number of genes up and down regulated in the four tissues of the three *Hmgn$^{-/-}$* mice lines compared to WT littermates. **(E-H)** Venn diagrams showing the overlap in the number of genes with altered expression in the tissues of each of the three genotypes examined. **(J-K)** Venn diagrams showing the overlap between the genes altered in the different tissues of each genotype.

Deng *et al* Figure 1

Deng *et al* Figure 2

A DHS distribution

B
- ■ Lost DHSs in *Hmgn1⁻/⁻n2⁻/⁻*
- ■ Gained DHSs in *Hmgn1⁻/⁻n2⁻/⁻*
- □ Retained DHSs in *Hmgn1⁻/⁻n2⁻/⁻*

C DHSs at H3K4me1 (non H3K4me3)

D DHSs at H3K4me1 (non H3K4me3)

E DHSs at H3K27ac (non H3K4me3)

F DHSs at H3K4me3

G

DHSs overlapping with H3K4me1 ■ DHSs overlapping with H3K4me3

Deng *et al* Figure 3

A

Hours after induction: 6, 4, 2, 1, 0.5

Higher *in Hmgn1^{-/-}n2^{-/-}*

Genes (left to right): * TNFAIP3, * CCL2, * DSCR1, * ZFP36, * NFKBIA, * IER3, GADD45B, * MAIL, * JUN, CTGF, * AXIN1, * GEM, * HBEGF, FOSL1, * CYR61, * KIF6, * MYC, TRIB1, * DUSP6, * JUNB, * CCNL1, * PLAU, CSRNP1, ATF3, NR4A1, NR4A2, MCL1, SRF, PGK1, DUSP1, SLC2A3, EGR3, DDIT3, GUSB, GAPDH, DUSP5, CCNA2, NR4A3, PMAIP1, EGR1, FLG, * SGK, * FOSB, * IL6, CEBPD, * FOS, GBP1

Log$_2$ (Induction ratio) — scale from 1 (green) to -1 (red)

Lower *in Hmgn1^{-/-}n2^{-/-}*

Control genes

B

Ccl2 — Nano-string signal vs Hours; WT (black), *Hmgn1^{-/-}n2^{-/-}* (red)

C

Il6 — Nano-string signal vs Hours; WT (black), *Hmgn1^{-/-}n2^{-/-}* (red)

D

DHS overlapping with H3K4me1 (pink); DHS overlapping with H3K4me3 (blue)

Genes: *Ccl2*
WT_1_DHS [0.1-1.0]
WT_2_DHS [0.1-1.0]
*Hmgn1^{-/-}n2^{-/-}*_1_DHS [0.1-1.0]
*Hmgn1^{-/-}n2^{-/-}*_2_DHS [0.1-1.0]
WT_H3K4me1 [0-1.5]
*Hmgn1^{-/-}n2^{-/-}*_H3K4me1 [0-1.5]
WT_H3K4me3 [0-0.5]
*Hmgn1^{-/-}n2^{-/-}*_H3K4me3 [0-0.5]

E

Hsp70 — Fold induction vs Minutes; WT (black), *Hmgn1^{-/-}n2^{-/-}* (red); *

F

DHS overlapping with H3K4me3 (blue)

Genes: *Hspa1b*, *Hspa1a*
WT_1_DHS [0.1-2.5]
WT_2_DHS [0.1-2.5]
*Hmgn1^{-/-}n2^{-/-}*_1_DHS [0.1-2.5]
*Hmgn1^{-/-}n2^{-/-}*_2_DHS [0.1-2.5]
WT_H3K4me1 [0-1]
*Hmgn1^{-/-}n2^{-/-}*_H3K4me1 [0-1]
WT_H3K4me3 [0-5]
*Hmgn1^{-/-}n2^{-/-}*_H3K4me3 [0-5]

Deng *et al* Figure 5

Table 1. Phenotypes detected in *Hmgn1$^{-/-}$*, *Hmgn2$^{-/-}$* and *Hmgn1$^{-/-}$n2$^{-/-}$* mice

Screen	Test	Phenotypes		
		Hmgn1$^{-/-}$	*Hmgn2$^{-/-}$*	**Hmgn1$^{-/-}$n2$^{-/-}$*
Energy Metabolism	Body mass	No [#]	Reduced (-)	Reduced (--)
	Fat content	No	Reduced	Reduced
	Indirect calorimetry	No	Hyperphagia (+)	Hyperphagia (++)
		No	Increased food intake (+)	Increased food intake (++)
		No	Higher respiratory exchange ratio	Higher respiratory exchange ratio
		No	No	Increased energy expenditure
Eye	Eye morphology	No	No	Higher number of the main blood vessels
	Eye size	No	No	Increased eye axial length
		No	No	Decreased corneal thickness
Clinical Chemistry	Clinical Chemistry (Fasting values)	Not measured	Elevated glucose, triglyceride, NEFA and non-HDL in females	Decreased glucose and cholesterol in males. Increased triglyceride, glycerol and NEFA in females
	Clinical Chemistry (Ad libitum fed values)	No	No	Lower albumin and alpha-amylase
		No	No	Higher triglyceride
		No	No	Higher cholesterol and calcium in females
	IpGTT	No	No	Increased basal fasting glucose in females
		No	No	Decreased AUC 30-120 in females
	Insulin (Fasting values)	Not measured	No	Lower plasma insulin
Hematology	Hematology	No	Elevated platelet count	Microcytic blood cell count without anemia
		No	Decreased platelet volume in males	Increased frequency of large platelets
Immunology	Main leukocyte subsets	No	No	Higher frequencies of T cells, NK cells and NKT cells
	T lymphocyte subsets	Lower CD4+/CD8+ ratio	No	Higher % of CD4+ T cells. Lower % of CD8+ T cells
	B lymphocyte subsets	No	No	Lower % of IgD+ B cells
		No	No	Lower % of MHC2+ B cells
		No		Higher % of IgD-IgM+CD23+CD21+ cells
		No	Higher % of CD11b+ cells	Lower % of IgD+IgM+CD23+CD21- cells
	Monocyte subsets	No	Lower % of CD11c+ Ly6C- cells	Lower % of CD11c+ Ly6C intermediate cells
		No	No	Lower % of CD11c+ Ly6C high cells
		No	No	Lower % of Ly6C high cells
		No	No	Higher % of Ly6C intermediate cells
	NK cell subsets	No	Lower % CD11c+ cells	Lower % of CD11c+ cells

*see Supplemental Table S6. # no phenotype seen

Functional compensation among HMGN variants modulates the DNase I hypersensitive sites at enhancers

Tao Deng, Z. Iris Zhu, Shaofei Zhang, et al.

Supplemental Material	http://genome.cshlp.org/content/suppl/2015/07/13/gr.192229.115.DC1.html
P<P	Published online July 8, 2015 in advance of the print journal.
Accepted Manuscript	Peer-reviewed and accepted for publication but not copyedited or typeset; accepted manuscript is likely to differ from the final, published version.
Creative Commons License	This article is distributed exclusively by Cold Spring Harbor Laboratory Press for the first six months after the full-issue publication date (see http://genome.cshlp.org/site/misc/terms.xhtml). After six months, it is available under a Creative Commons License (Attribution-NonCommercial 4.0 International), as described at http://creativecommons.org/licenses/by-nc/4.0/.
Email Alerting Service	Receive free email alerts when new articles cite this article - sign up in the box at the top right corner of the article or **click here.**

To subscribe to *Genome Research* go to:
http://genome.cshlp.org/subscriptions